Fabrication of a Novel Microsensor Consisting of Electrodeposited ZnO Nanorod-Coated Crossed Cu Micropillars and the Effects of Nanorod Coating Morphology on the Gas Sensing

4 AUTHORS, INCLUDING:

Yao-Tien Tseng
National Central University
1 PUBLICATION   **5** CITATIONS

SEE PROFILE

Jing-Chie Lin
National Central University
216 PUBLICATIONS   **1,757** CITATIONS

SEE PROFILE

Yean-Ren Hwang
National Central University
**34** PUBLICATIONS   **385** CITATIONS

SEE PROFILE

Fabrication of a Novel Microsensor Consisting of Electrodeposited ZnO Nanorod-Coated Crossed Cu Micropillars and the Effects of Nanorod Coating Morphology on the Gas Sensing

Yao-Tien Tseng,[†] Jing-Chie Lin,*,[†] Yong-Jie Ciou,[‡] and Yean-Ren Hwang[‡]

[†]Institute of Materials Science and Engineering and [‡]Department of Mechanical Engineering, National Central University, Taoyuan 32001, Taiwan

ABSTRACT: A novel microsensor, consisting of crossed Cu micropillars coated with ZnO nanorods, was fabricated by electrochemical methods for detecting gas in a small space. The Cu micropillars (80 μm diameter, 10 mm long) were prepared by microanode-guided electroplating (MAGE) on the periphery of a square copper pad (dimensions 5.0 mm × 5.0 mm × 1.0 mm). The micropillars were electrochemically coated with a 500 nm thick layer of ZnO nanorods deposited from a bath containing 2.0 mM zinc chloride and H_2O_2 varying in 5, 10, 15, and 20 mM. Two ZnO-coated pillars were crossed to form a microsensor by approaching the Cu pads below, which was adhered to an alumina substrate with silver paste and connected to conducting wires for measurement. The morphology of the coating of ZnO nanorods, which was found to be determined by the concentration of H_2O_2 in the bath, influenced the gas sensing. The morphology of the coating was characterized by scanning electron microscopy; the structural analysis was carried out by X-ray diffraction and high-resolution transmission electron microscopy (HRTEM); the surface analysis was carried out by X-ray photoelectron spectroscopy; and the defects were determined with photoluminescence (PL) spectra. We thus investigated the effect of the morphology of the coating on the sensing properties by introducing a stream of gases varying in CO/air ratios to understand the sensing mechanism of the microsensor.

KEYWORDS: ZnO, single crystalline, real-time guided continuous microelectroplating, microsensor, gas sensing
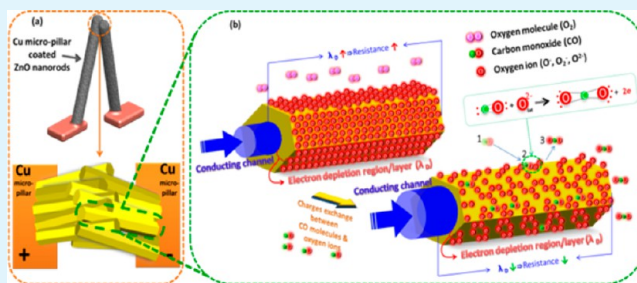
1. INTRODUCTION

Microanode-guided electroplating (MAGE) provides a convenient and economic route to fabricate microstructures with its operation in ambient open-air conditions rather than in a cleanroom.[1−3] In our previous study, we adopted the MAGE process to prepare a microthermocouple consisting of a pure Cu pillar in conjunction with another 47Ni/53Cu alloying pillar to demonstrate satisfactory thermal measurement from 20 to 70 °C with good precision and sensitivity.[4] Encouraged by this work, we attempted to develop, by a simple electrochemical process, a novel steric microsensor based on a crossed structure of two Cu micropillars coated with a metal oxide.

Recently, semiconducting metal oxides, such as ZnO, SnO_2, and TiO_2, have drawn immense attention owing to their tunable electronic and optoelectronic properties and potential applications in electronic and optoelectronic devices.[5,6] In the past decade, nanostructures of many of these oxides were considered for potential use in gas sensing because of their slow rate of electron/hole recombination and large surface area.[7−10] ZnO has received much attention because of its abundance in the earth's crust, low cost, and nontoxic properties, along with a wide band gap of 3.37 eV, a large exciton binding energy of 60 meV at room temperature, and excellent chemical and thermal stabilities. There are a number of reports published with regard to the sensing behavior of ZnO, specifically that of one-

dimensional nanostructures of ZnO for the detection of gases, such as oxygen, carbon monoxide, ethanol, NO_2, and volatile organic compounds.[11,12] However, only a few articles focus on the manufacturing of a complete sensing system based on ZnO or have discussed the performance of such a system in gas sensing applications. ZnO-based sensors are usually constructed on a planar insulating substrate (i.e., silicon wafer or alumina) on which conductive Au electrodes are deposited previously on an oxide layer (i.e., SiO_2) present on the silicon or Al_2O_3 substrate. A layer of ZnO nanostructures, which act as functional materials for sensing, was coated on the top surface of sensors by physical vapor deposition,[13] chemical vapor deposition,[14] atomic layer deposition,[15] chemical bath deposition, or hydrothermal process,[16,17] etc. Many researchers have observed that the sensitivity, selectivity, and stability of the sensor were determined by the morphology and structure of the functional materials, which in turn depended on the techniques of deposition. An electrochemical technique was considered as an economic and convenient method to fabricate microscale features; however, sensors coated with ZnO nanostructures prepared by the electrochemical process have
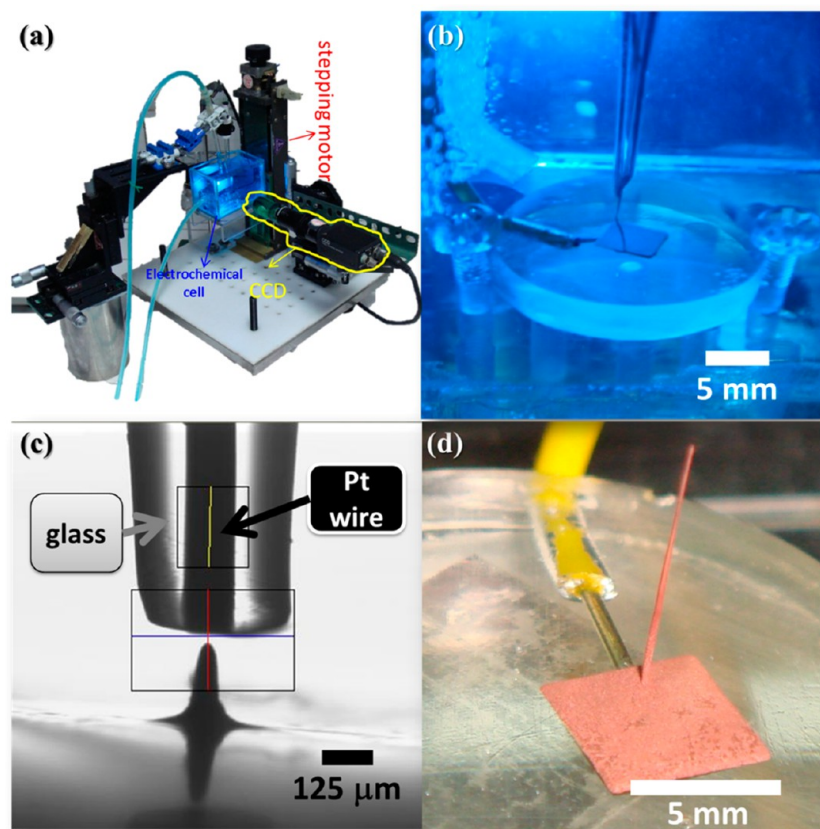
Figure 1. (a) MAGE monitoring and controlling system, (b) electrochemical cell, (c) the constant separation (of 25 μm) between the microanode and the top of the Cu micropillar, and (d) a micropillar of 10 mm in length.

seldom been reported. In the present work, we attempted to prepare a microsensor to detect the gas, which is applicable for a narrow space. Instead of a common planar sensor coated with a thin film of ZnO nanostructures, the novel microsensor we have prepared is a cross-shaped device obtained by the mechanical contact of two Cu micropillars coated with ZnO nanorods, by approaching the separated Cu pads where both ZnO-coated Cu micropillars were grown to make sure there is a firm contact of the cross point. The Cu pads were adhered to an alumina substrate with silver paste and were then connected with conducting wires to a digital multimeter to carry out the sensing measurement. The coating of ZnO rods acted as the functional sensing material, and the Cu micropillars and the Cu pads were the conducting electrodes. This steric microsensor was specially designed for use in a narrow space (i.e., in tubing systems) to detect the leakage of the gas and to monitor the degree of vacuum and variation in the concentration of the gases.

2. EXPERIMENTAL PROCEDURES

2.1. Fabrication of Copper Micropillars on Cu Pads by the Continuous MAGE Monitoring and Controlling System. Prior to preparing the ZnO coating on pillars, Cu micropillars were first prepared by MAGE via a real-time monitoring and controlling system on the periphery of a copper pad (5.0 mm × 5.0 mm × 1.0 mm, 99.9%, Alfa Aesar) in a bath of 0.5 M copper sulfate ($CuSO_4$, reagent grade, 99% Sigma-Aldrich).[1-3] The square copper pad (5.0 mm × 5.0 mm × 1.0 mm, metals basis) was ground sequentially with emery papers of various degrees of roughness up to 2000 grit and polished

with a paste containing 0.5 μm powders of alumina to obtain a smooth and bright surface before immersion into the bath for the electrochemical deposition. Platinum wire (125 μm in diameter, metals basis, 99.99%, Alfa Aesar) mounted in a glass tube (0.25 mm in diameter) was used as a microanode. Electrochemical deposition was conducted at 3.4 V across the microanode and copper substrate to electroplate a copper micropillar (80 μm in diameter and 10 mm in length) via the homemade continuous MAGE monitoring and controlling system, as shown in Figure 1(a), which is comprised of an electrochemical cell driven (as shown in Figure 1(b)) by a stepping motor on the table and a charge-coupled device (CCD 97C, Sony, Japan) to monitor and control the deposition process. A constant separation (of 25 μm) was maintained between the microanode and the top of the Cu micropillar (as demonstrated in Figure 1(c)) to maintain the steady growth of the micropillar. Once the micropillar grew to 10 mm determined by the real-time monitoring and controlling system in the experimental setup (as depicted in Figure 1(d)), it was removed from the electrochemical cell and was cleaned and dried with a stream of nitrogen gas. Then, the sample was stored in a desiccator before electrochemically coating with the ZnO nanorods.

2.2. Electrochemical Coating of ZnO Nanorods on the Cu Micropillar. The Cu micropillars obtained in Section 2.1 were immersed in another electrochemical cell, which was filled with solutions of 2.0 mM $ZnCl_2$ (anhydrous, reagent grade, 99.99% Sigma-Aldrich) containing hydrogen peroxide (35 wt % in H_2O, Sigma-Aldrich) at various concentrations ranging from 5 to 20 mM. The pH of the baths was determined by a pH

Table 1. Parameters of the Baths Used for the Electrochemical Coating of ZnO and the Characteristics of the Nanorods in the Coatings

conditions of different baths				nanorods obtained from different baths				
				length (L) (nm)		diameter (D) (nm)		
concentration of H_2O_2 in the bath (mM)	initial pH of the bath	solution resistivity (Ω cm)	charge density consumed (C/cm^2)	average	std. dev.	average	std. dev.	aspect ratio (L/D)
5	7.00	72.46	1.37	78.8	8.3	36.5	8.4	2.1
10	7.03	64.94	2.84	164.8	14.6	68.7	13.2	2.4
15	7.06	59.88	4.22	341.8	25.9	105.2	17.0	3.3
20	7.08	54.95	5.61	629.8	31.6	168.2	21.7	3.8
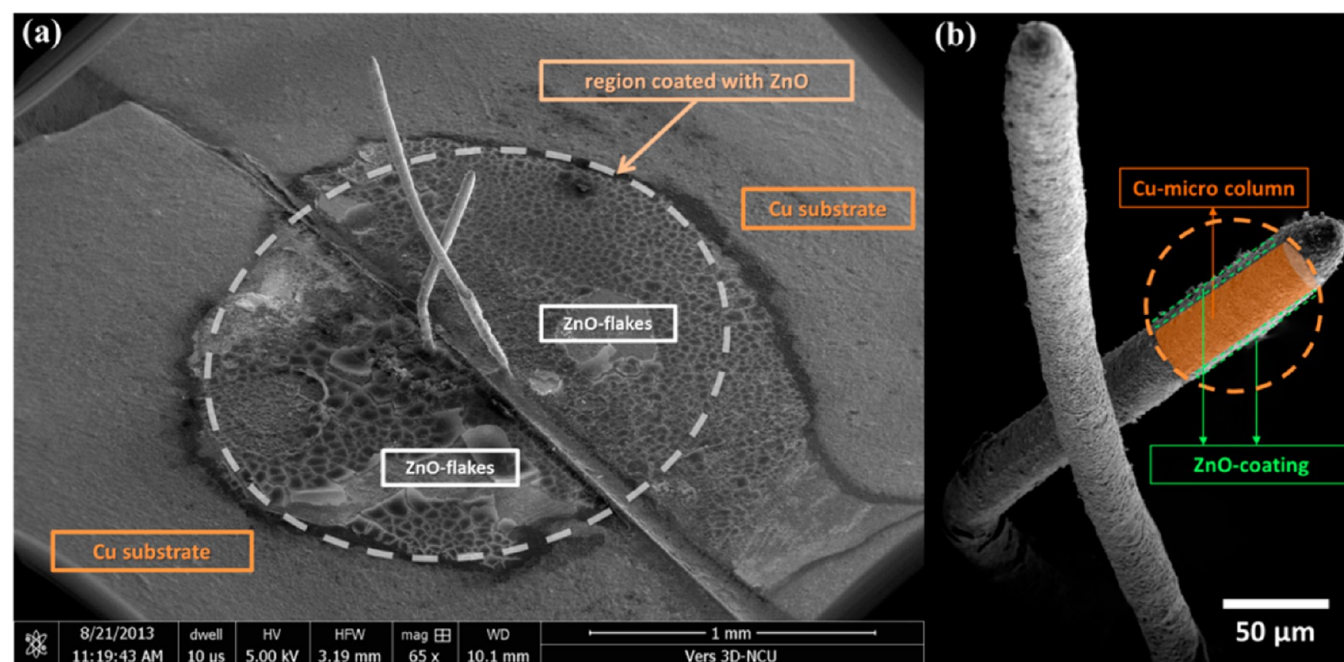
Figure 2. (a) SEM image of a crossed pair of ZnO-coated copper pillars on two separated Cu pads covered with ZnO coating in the microsensor and (b) schematic representation of one of the magnified micropillars indicating the ZnO coating.

meter (Cyber Scan pH 510, Eutech, Singapore), and the specific resistivity of the bath was measured by a conductivity meter (Cyber Scan CON 110, Eutech, Singapore). The bath was controlled at 80 °C thermostatically to conduct the electrochemical process in which the Cu micropillar was used as the cathode; a hallow cylinder made of platinum mesh (25 mm in diameter with 15 mm in height) wrapped around the cathode was used the anode; and a commercial silver/silver chloride electrode (Ag/AgCl/3.0 M KCl with 0.210 V$_{SHE}$) in connection with the salt bridge capillary was used as the reference electrode in which the separation between the capillary tip and the cathode (i.e., Cu micropillar) surface was maintained at around 1.0 mm. The electrochemical deposition was carried out potentiostatically at −1.0 V for 20 min through a potentiostat (PGSTAT30, Autolab, Netherlands), and the current was measured. The parameters of baths used for the electrochemical coating of ZnO nanorods are summarized in Table 1. The as-deposited electrochemical coatings were subjected to morphological observation and analyses.

2.3. Morphology, Crystalline Structure, and Characterization of the ZnO Coating. The morphologies of the ZnO coating on the Cu micropillar were observed by field-emission scanning electron microscopy (FE-SEM, Nova Nano SEM 230, FEI, USA), and the size of the nanostructures was estimated using a software associated with the SEM. The chemical state of the coating and the semiquantitative elemental analysis were carried out using X-ray photoelectron spectroscopy (XPS, VG-Scientific Sigma Probe spectrometer, UK). Prior to XPS analysis, we sputtered the surface of the coating with Ar ions (5 keV) for 30 s to remove the air contaminated layer (around 3 nm in thickness). Trace amounts of the ZnO coating were detached from the coated micropillar, and they were filled in a zero background holder for the determination of its crystalline structure with X-ray diffraction (XRD, D8A X-ray diffractometer, Bruker, Germany). The ZnO-coated micropillar was treated by a dual beam focus ion beam (FIB, VERSA 3D, FEI, USA) to obtain a sample containing the interface between the ZnO coating and the pillar substrate. The sample moved electrostatically to a carbon-coated 200-mesh copper grid for examination by high-resolution transmission electron microscopy (HRTEM, JEOL JEM-2100 (Tokyo, Japan)) at an acceleration voltage of 200 kV. The optoelectronic properties of the ZnO-coated Cu micropillar were examined at room temperature using a photoluminescence spectrometer (PL, FluoroMax-3, Jobin-Yvon, Japan) with a 325 He−Cd laser as the source of excitation with emission wavelengths in the range 370−500 nm.

11426

dx.doi.org/10.1021/am5019836 | ACS Appl. Mater. Interfaces 2014, 6, 11424−11438
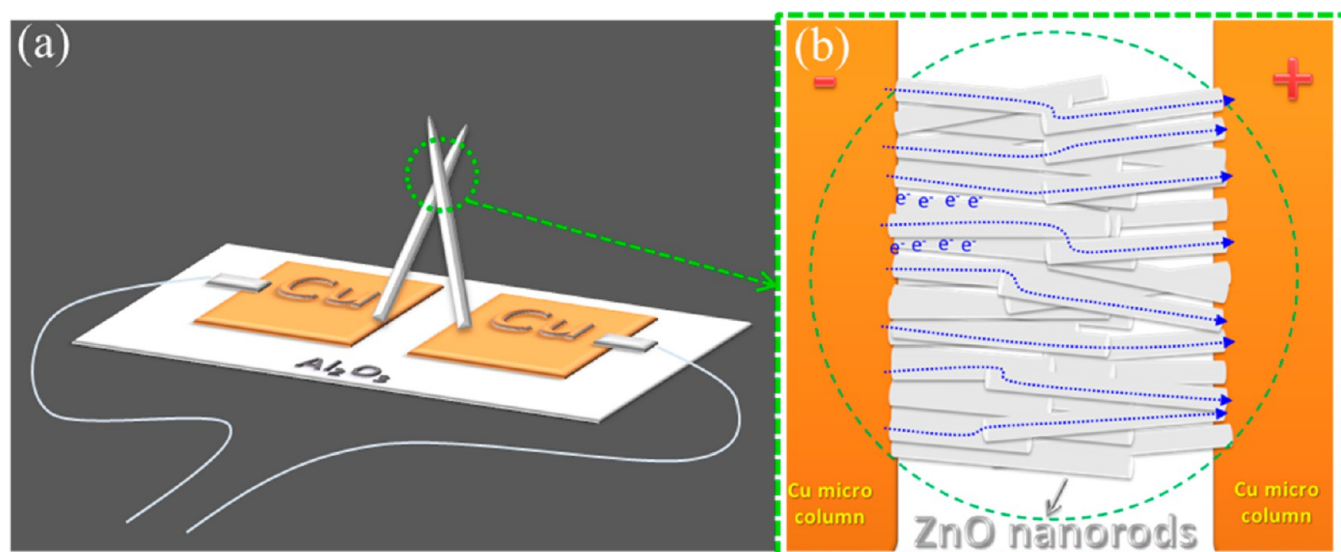
Figure 3. (a) Schematic cross-shaped microsensor constructed with a pair of ZnO-coated Cu micropillars grown upon separated Cu pads on an alumina substrate connected with conductive Ag wires linking up to a direct current power source loaded at a constant voltage. (b) Schematic presentation of the cross point shown in (a) at a higher magnification to illustrate the transfer of electrons from the negative pole of the Cu micropillar through its ZnO coating via the crossed contact and along the ZnO coating to reach the positive Cu micropillar at a constant voltage load (of 5 V) from a direct current power source.
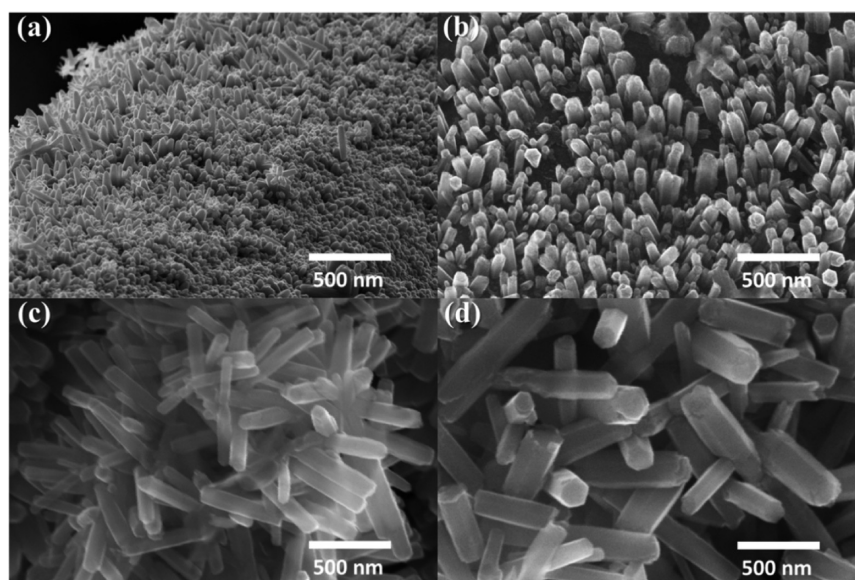
Figure 4. SEM images of the ZnO nanorods electrochemically deposited on the copper micropillars from a bath containing 2.0 mM $ZnCl_2$ with H_2O_2 concentrations of (a) 5 mM, (b) 10 mM, (c) 15 mM, and (d) 20 mM.

2.4. Assembly of the Sensor and Its Operation. A pair of the ZnO-coated Cu micropillars along with their bases (i.e., Cu square pads) was placed on the surface of an alumina substrate. The alumina substrate was placed on a stage. One of the ZnO-coated micropillars was fixed on the alumina by fixing its Cu square pad with silver paste, while the other micropillar was moved to approach the fixed one by pushing its base with a piece of glass tip driven under the precise control of a micrometer step motor. The approaching motion was monitored with a set of CCD (97C, Sony, Japan) in combination with an optical lens (FM-200, Proximity, USA). As soon as the second ZnO-coated pillar came into contact with the first one, the two pillars gave rise to a crossed structure. However, further contact would lead to the bending of the micropillars. At the moment the two pillars with a cross shape bend slightly, we glued the Cu square pad of the second micropillar to the alumina substrate immediately to ensure the intimate contact of the micropillars. The system consisting of these two ZnO-coated pillars with a crossed structure was connected with conducting silver wires at the base of the Cu square pads to accomplish a steric gas microsensor, as depicted in Figure 2(a). Figure 2(b) displays a schematic representation of one of the micropillars in the cross with the ZnO coating. This cross-shaped gas sensor was heated in a furnace at 450 °C under an air atmosphere for 12 h to ensure a stable measurement of the electric resistance prior to gas sensing.

Sensors based on semiconducting oxides are mainly employed to detect target gases through redox reactions

between the target gases and the oxide surface to result in a prominent change in electric resistance of the sensing materials.[18,19] A schematic structure of the cross-shaped sensing system used presently is depicted in Figure 3(a). The transfer of electrons inside the sensing system when the two ZnO-coated micropillars were loaded with a constant voltage (i.e., 5 V) from a direct current power source (digital multimeter, 34410A, Agilent, USA) is exhibited in Figure 3(b). The electric resistance, which was in the scale of mega ohms (10^6 Ω), could be used as an indication of the intimate contact between the two ZnO-coated micropillars within the sensor. Sensing measurements of the semiconducting oxides, such as ZnO nanostructures, should be conducted at a temperature ranging from 100 to 400 °C. In this work, the sensor was placed in a tube furnace (Lindberg Blue M, USA) in which the temperature was controlled in the range 100−400 °C, and the relative humidity was controlled at 25%−30%. Then, a stream of CO/air gas mixture was made to flow at various rates to set the CO concentrations at 5, 10, 15, 20, and 25 ppm. Air and CO were supplied in bottles (Air Products San Fu Co. Ltd., Taiwan), and their flow rates were controlled by means of two mass flow controllers (New-flow, Taiwan). The digital multimeter (Agilent 34410A) was used to carry out the $I−V$ measurement and data acquisition to calculate the electric resistance, and the sensitivity of the sensor was estimated. At least four experimental runs were carried out to ensure the reproducibility of the data and to obtain average values of the sensitivity and their standard deviations. The sensitivity (denoted with S) was defined as a ratio of the electrical resistances (i.e., R_a/R_g) for reducing gases and R_g/R_a for oxidizing gases. R_a and R_g represent the steady-state resistances of the gas sensor operated in air and in the test atmosphere (in which the target gas is mixed with air), respectively.

3. RESULTS AND DISCUSSION

3.1. Surface Morphology of the ZnO Coatings as a Function of the H_2O_2 Concentration in the Bath.
Figure 4 show the SEM surface morphologies of the ZnO coatings on the Cu micropillar as a function of H_2O_2 concentration in the electrochemical bath. As seen in Figure 4, all the coatings were composed of nanorods. However, these nanorods were different in sizes, which were determined by the concentration of hydrogen peroxide in the bath. In addition to the diameter, the length of the nanorods increased with an increase in the peroxide concentration from 5 to 20 mM. The dimensions of the nanorods were estimated by the software associated with the SEM, and the diameters and lengths for the nanorods are listed Table 1. It is evident that the diameter increased from 36.5 to 168.2 nm, and the length increased from 78.8 to 629.8 nm with an increase in the H_2O_2 concentration from 5 to 20 mM. The aspect ratio (L/D) of the nanorods increased from 2.1 to 3.8 with an increase in the H_2O_2 concentration. This implied that the growth rate of the length is more rapid than that of the diameter for the nanorods deposited electrochemically.

For the electrochemical coating of ZnO conducted at −1.0 V (vs Ag/AgCl), the current density in the different baths containing various concentrations of H_2O_2 was monitored and recorded against time, as shown in Figure 5. In Figure 5, the negative values of the current density indicate a cathodic reaction in response to the reduction reactions. The current density in absolute values decreased with time. The higher the concentration of hydrogen peroxide, the higher the absolute
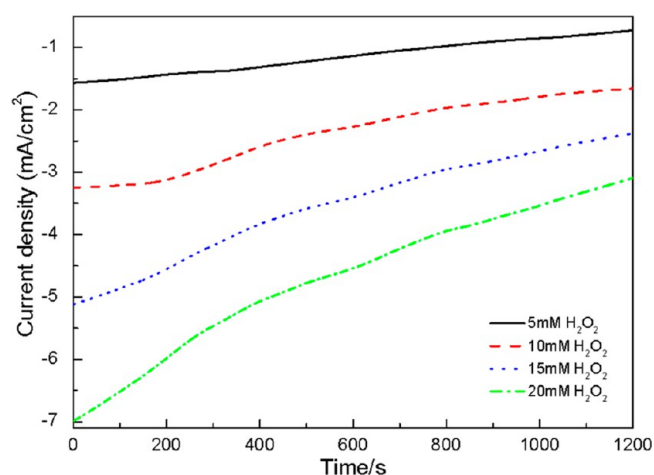

Figure 5. Current density as a function of time measured during the electrochemical deposition of ZnO nanorods on the Cu micropillar in the baths containing 2.0 mM $ZnCl_2$ and 5, 10, 15, and 20 mM hydrogen peroxide.

value of the current density was. Referring to the data listed in Table 1, we found that the initial pH and the specific resistivity of the bath depended on the concentration of H_2O_2. The slight increase in pH may have resulted from the degradation of H_2O_2 to produce a diluted concentration of hydroxyl ions (OH^-). The slight decrease in the specific resistivity is also ascribed to an increase in the ionic species, i.e., the small concentration of hydroxyl ions originating from the spontaneous decomposition of hydrogen peroxide.[20] By integrating the current density versus time plot (in Figure 5), we obtained the charge density consumed in the electrochemical coating of ZnO. Comparing the charge density data listed in Table 1, the process performed in the bath containing concentrated H_2O_2 consumed a greater quantity of charges than the process performed in the bath with diluted H_2O_2. On the basis of this, we expected that greater amounts of ZnO would be coated on the Cu micropillar when the electrochemical coating is performed in a bath containing a higher concentration of H_2O_2, even though the concentration of $ZnCl_2$ is constant.

3.2. TEM and HRTEM Analysis of the ZnO Coatings.
TEM and HRTEM were employed to study in further detail the ZnO coating by observing the nanorods at higher magnifications and to examine the electron diffraction patterns to identify ZnO crystallography. Figure 6(a) shows the TEM bright-field image of the ZnO coating electrochemically deposited on the Cu micropillar from a bath containing 2.0 mM $ZnCl_2$ and 20 mM H_2O_2. The coating specimen was first coated with a film (1.2 μm) of Pt by electron beam deposition, and then another Pt layer (1.5 μm) was deposited by ion beam for protection against subsequent treatment with a focused ion beam to obtain a cross-sectional thin film, containing a ZnO coating/Cu micropillar substrate interface, with a thickness less than 100 nm. Evidently, the electrochemical ZnO coating belonged to a layer of the nanorod structure adhered on the Cu micropillar surface. The sizes of the nanorods evaluated from TEM images were consistent with those estimated from the SEM images, as indicated in Table 1. Figure 6(b) displays the TEM image of a single ZnO nanorod chosen from the ZnO coating layer shown in Figure 6(a). A local region was selected on the single ZnO nanorod specimen to be examined by HRTEM. The results obtained were similar irrespective of the region selected. Figure 6(c) shows the HRTEM image of the
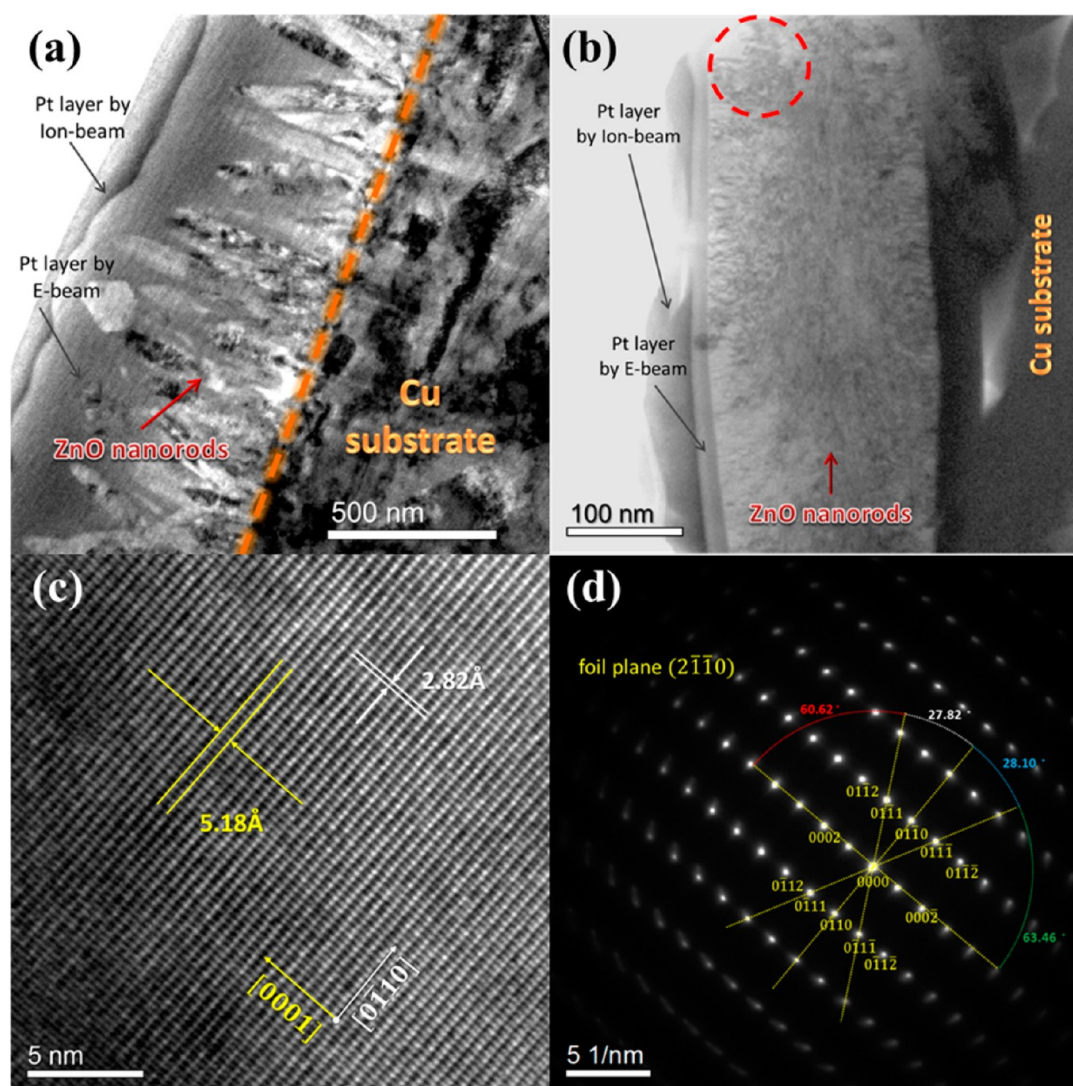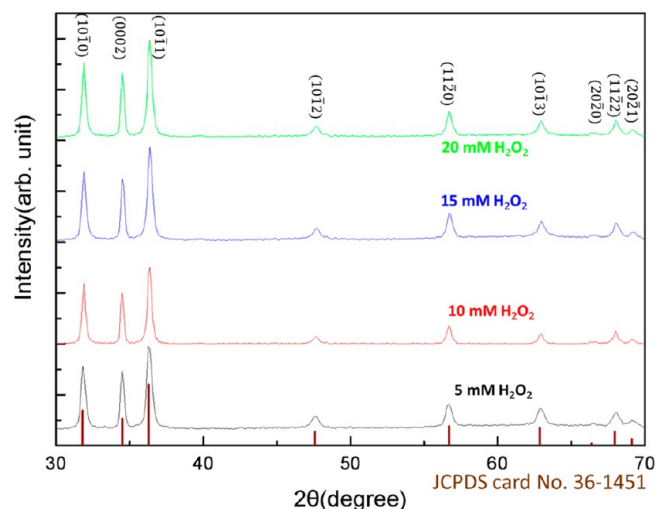
Figure 6. (a) TEM image of the ZnO coating electrochemically deposited on the Cu micropillar from a bath containing 2.0 mM ZnCl$_2$ and 20 mM H$_2$O$_2$. (b) TEM image of a single ZnO nanorod chosen from the ZnO coating layer shown in (a). (c) HRTEM image of the region of the ZnO nanorod marked with a circle in (b) with the zone axis along [0001]. (d) SAED pattern along the ($2\bar{1}\bar{1}0$) foil plane of the ZnO nanorod.

circular region marked on the single ZnO nanorod shown Figure 6(b) with the zone axis along [0001]. On the basis of the lattice fringes of this ZnO nanorod, we could evaluate the interplanar distance for the (0001) as 5.18 Å and for ($0\bar{1}10$) as 2.82 Å. Figure 6(d) shows the selected area electron diffraction (SAED) pattern of the ZnO nanorod along the ($2\bar{1}\bar{1}0$) foil plane, indicating that the ZnO nanorod belongs to the hexagonal wurtzite structure.[21]

3.3. XRD Patterns of the Various ZnO Coatings Removed from the Microsensors. Figure 7 shows the XRD patterns of the ZnO coatings detached by scratching the various samples of Cu micropillars. Three main strong peaks at ($10\bar{1}0$), (0002), and ($10\bar{1}1$) and a few minor weak peaks were observed, as shown in Figure 7. We identified that the ZnO coating exhibited the hexagonal structure of wurtzite (with the lattice constant a = 3.253 Å and c = 5.209 Å, JCPDS card No. 36-1451). After estimating the full width at half-maximum (fwhm) of the three main peaks, we plotted the fwhm as a function of the H$_2$O$_2$ concentration in the bath, as shown in Figure 8. The value of the fwhm decreased slightly with an increase in the concentration of H$_2$O$_2$ from 5 to 15 mM and

Figure 7. XRD patterns of the detached ZnO nanorods electrochemically deposited on the copper micropillar from baths containing 2.0 mM ZnCl$_2$ and 5, 10, 15, and 20 mM H$_2$O$_2$.
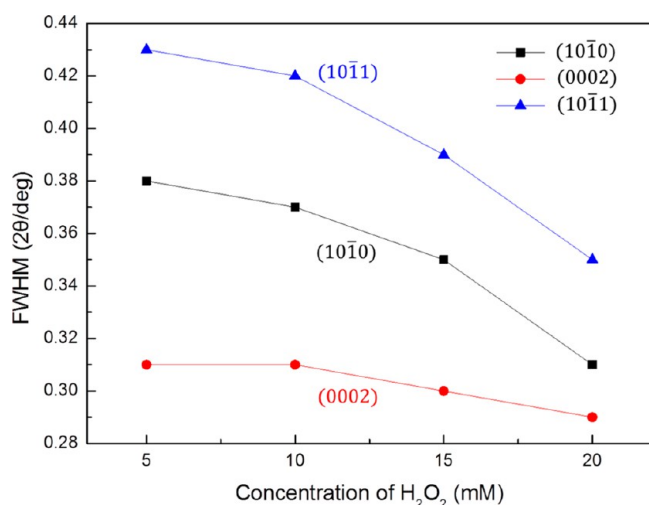
Figure 8. fwhm of the three main strong peaks from $(10\bar{1}0)$, (0002), and $(10\bar{1}1)$ planes of the ZnO coating shown in the XRD patterns of Figure 7.

then dramatically decreased with an increase in concentration from 15 to 20 mM. The lower the value of the fwhm, the more pronounced the crystallinity. Hence, the ZnO coatings electrochemically deposited from a bath containing higher H_2O_2 concentration (especially at 20 mM) showed better crystallinity. This confirmed the SEM observations of the ZnO

coatings shown in Figure 4. Comparing the size of the nanorods in Figures 4(a), (b), (c), and (d), the crystallinity of the nanorods deposited from the bath containing the more concentrated H_2O_2 was much better.

For estimating the ease of the electrochemical deposition and the residual stress remaining in the ZnO coating after the electrochemical coating on the Cu micropillar substrate, we compared the crystal structure of the coating and the substrate. Since ZnO nanorods belong to wurtzite ($a = 3.2458$ Å, $c = 5.2006$ Å) with the basal plane on (0002), their lattice constant (i.e., $a = 3.2458$ Å) was similar to that of the copper micropillar substrate (with $a = 3.6149$ Å in the face centered cubic structure). Similar lattice constants caused only a small mismatch of 10% at the ZnO coating/Cu micropillar substrate interface.[22] In other words, the deposition of the ZnO coating was relatively easy and resulted in only a small residual stress inside the coating. Thus, the adhesion of the ZnO coating on the copper substrate would be better than that on other substrates, such as the ordinary indium tin oxide (ITO)-coated glass used in conventional sensors.[23] Copper was chosen instead of silver or gold as the conducting electrode in the microsensing system in view of its lower cost, good electric conductivity, and convenient processability through the MAGE process to prepare micropillars.

3.4. XPS Analysis of the Various ZnO Coatings. The XPS analysis of the ZnO coating indicated the presence of O 1s, Zn 2p3, and Zn 2p1 peaks. This implies that only pure ZnO
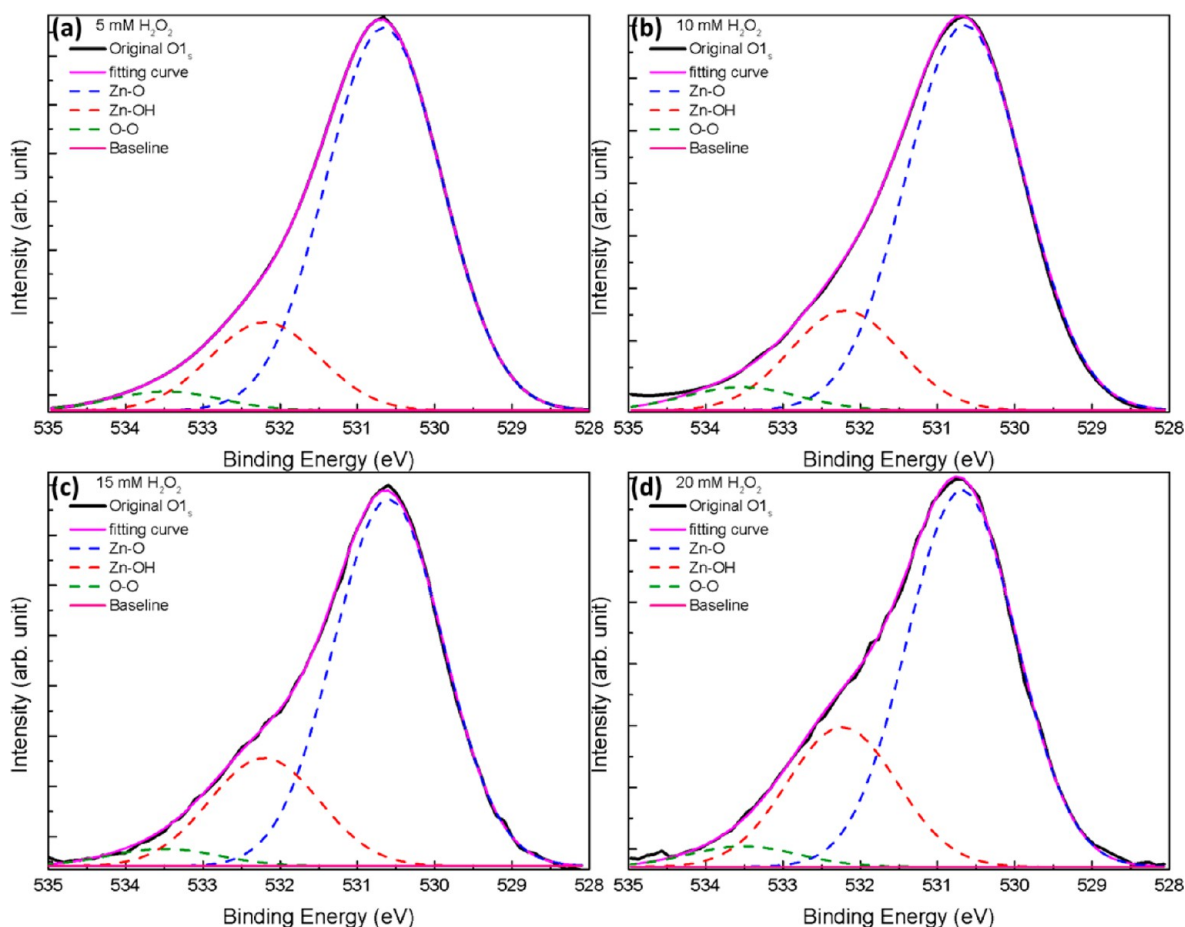
Figure 9. High-resolution XPS profiles and their deconvolution curves of O 1s from ZnO nanorods electrochemically deposited on copper pillars in the baths containing 2.0 mM $ZnCl_2$ with H_2O_2 concentrations of (a) 5 mM, (b) 10 mM, (c) 15 mM, and (d) 20 mM.
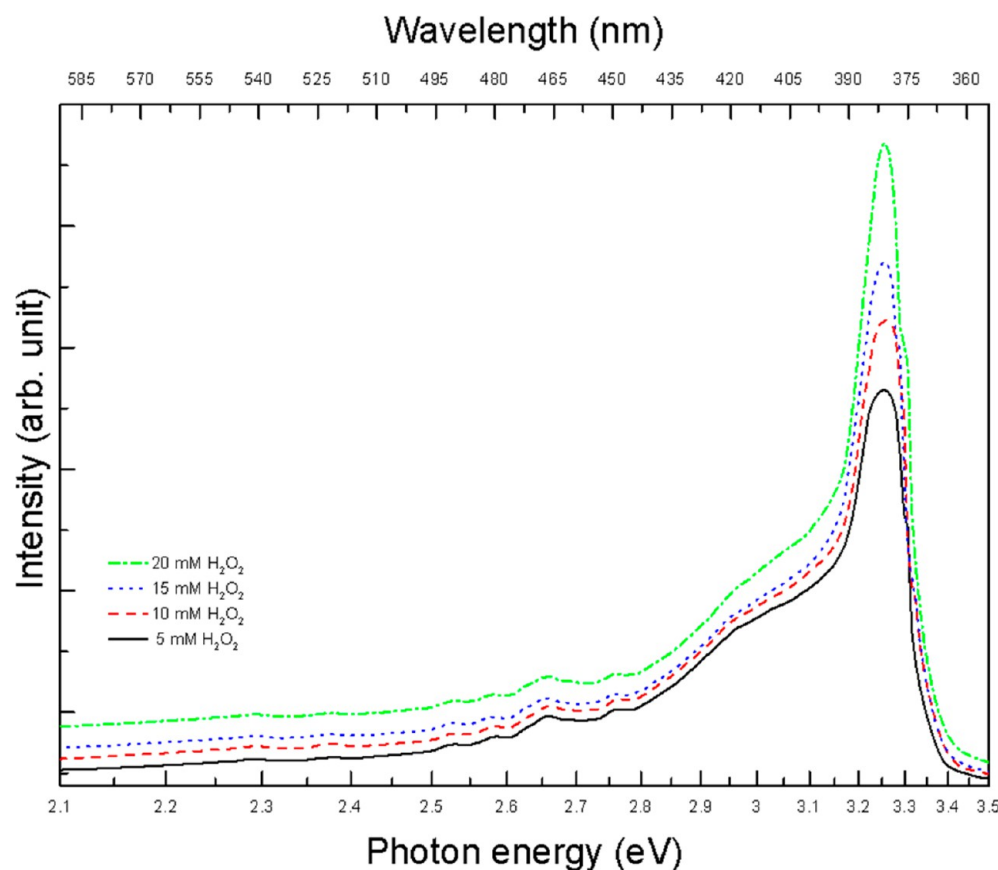
Figure 10. Photoluminescence spectra from the ZnO powders detached from the electrochemical coating obtained from a bath containing 2.0 mM ZnCl$_2$ with H$_2$O$_2$ concentrations of 5, 10, 15, and 20 mM.

was deposited on the surface. Figure 9 shows the O 1s XPS profile of the ZnO coatings obtained from baths containing (a) 5 mM, (b) 10 mM, (c) 15 mM, and (d) 20 mM H$_2$O$_2$. The spectra were obtained after cleaning the samples (at a rate of 1 Å/s) with an Ar ion gun for 30 s to remove any surface contamination from air-adsorbed impurities. The asymmetrical curves of O 1s implied the existence of a few chemicals with different binding energies. The O 1s peaks were deconvoluted into three Gaussian curves in response to three different oxygen moieties (i.e., ZnO, Zn(OH)$_2$, and adsorbed O$_2$ or H$_2$O) in the ZnO coating. The peak positions of the three Gaussian curves were centered at 530.5, 531.6, and 532.6 eV, which could be attributed to Zn−O, Zn−OH, and the oxygen coming from water chemisorbed on the surface of ZnO, respectively.[24,25] To estimate the quantitative composition of the coating, we integrated each Gaussian curve and divided the value by the total area of the overall asymmetrical peak. The area ratio of each component should be proportional to its concentration. In the case of the electrochemical reaction conducted in a bath containing dilute hydrogen peroxide (i.e., 5 mM H$_2$O$_2$), the resultant coating consisted of 77.64% ZnO, 15.88% Zn−OH, and 6.48% of oxygen from chemisorbed water. With an increase in the concentration of H$_2$O$_2$ from 10, 15, and up to 20 mM in the bath, the content of ZnO in the coatings slightly decreased (i.e., 75.65%, 73.97%, and 70.33%, respectively), whereas the content of Zn−OH increased (i.e., 18.96%, 22.22%, and 25.80%, respectively), with the chemisorbed water content remaining nearly constant (i.e., 5.39%, 3.81%, and 3.87%, respectively). The slight increase in the Zn−OH content along with the decrease in ZnO in the coatings may be ascribed to the
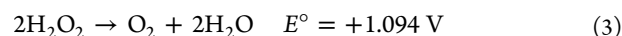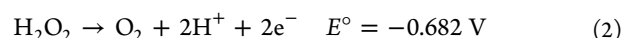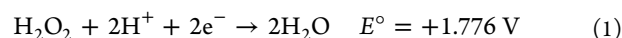
superior formation of hydroxide ions assisting the formation of zinc oxide in the baths containing concentrated H$_2$O$_2$. The mechanism is discussed later (in section 3.6).

3.5. PL Spectra of the ZnO Nanorods. With regard to gas sensing, the nanostructured ZnO coatings may provide better sensing capabilities because of their huge surface to volume ratios. As shown in Figures 4 and 6, the electrochemical coatings of ZnO on the Cu micropillars are comprised of nanorod structures, which are expected to show good sensing capabilities. A typical gas sensor made of ZnO principally uses the change in the electrical resistance, which occurs on contact with the gas to be detected in comparison to the resistance shown in the presence of atmospheric oxygen. It is known that the electronic properties of ZnO are determined by its nonstoichiometry and crystal defects. Both nonstoichiometry and defects in the ZnO nanorods of the coating may influence the electrical resistance and, therefore, the sensitivity. According to previous reports, the intrinsic defects of ZnO can be categorized as zinc interstitial (Zn$_i$), zinc vacancy (V$_{Zn}$), oxygen interstitial (O$_i$), oxygen vacancy (V$_O$), oxygen antisite (O$_{Zn}$), and Zn antisite (Zn$_O$). Among these six defects, Zn$_O$ shows a low probability of formation because of its high formation energy.[24,26] Zn$_i$ and V$_O$ facilitate the formation of free electrons (i.e., these are donors) in the ZnO crystal, whereas, V$_{Zn}$, O$_i$, and O$_{Zn}$ consume free electrons (i.e., these act as acceptors).[26,27] The presence of a higher number of Zn$_i$ and V$_O$ than V$_{Zn}$, O$_i$, and O$_{Zn}$ may make the ZnO nanorods n-type semiconductors.

Gas sensing capability of ZnO nanorods produced by electrochemical processes has been seldom reported. The effect of the composition and crystallinity of the ZnO nanorods

on the sensitivity of the electrochemical coatings is the focus of the present work. PL analysis is a useful technique to explore the defects present in the ZnO crystals. Figure 10 shows the PL spectra of the ZnO powders detached from the electrochemical coating. The coatings were obtained from baths containing 2.0 mM $ZnCl_2$ along with various concentrations of H_2O_2 (5, 10, 15, and 20 mM). A very strong and broad emission was observed ranging from 2.9 to 3.3 eV, which was accompanied by relatively weak emissions in the visible region ranging from 2.5 to 2.8 eV. The strongest PL emission (at 381 nm and 3.25 eV) shown in Figure 10 may be ascribed to the near band edge (NBE) transition (resulting from the excitonic recombination[28,29]) and radial recombination in the direct band gap of ZnO. The emission of visible light could have resulted from the primary defects in ZnO, such as oxygen vacancies (V_O)[30,31] and interstitial zinc atoms (Zn_i).[32−34] By checking the PL spectra reported in the literature,[24] we found that the intensity of the emissions in the visible region was less than that observed for ZnO nanoflakes produced by a hydrothermal process. From this, we inferred that the ZnO nanorods formed in the coatings by the electrochemical process contain a lesser number of defects than those produced by the hydrothermal process. It is worth noting that the intensity of the PL emissions increases with an increase in the H_2O_2 concentration in the bath used for the electrochemical coating. In conjunction with the SEM images in Figure 4, we infer that the larger ZnO nanorods are responsible for the stronger NBE emissions. This is in agreement with the results reported in the literature.[35−38] An increase in the intensity of the weak visible region emission with an increase in the H_2O_2 concentration in the bath used for the electrochemical coating could be ascribed to the increase in the intrinsic defects.

3.6. Mechanism Operating Behind the Influence of the H_2O_2 Concentration in the Bath on the Morphology of the ZnO Nanorods. The effect of H_2O_2 concentrations used in the electrochemical bath on the morphology of the ZnO nanorods could be understood with the electrochemical kinetics. It is well-known that H_2O_2 is an unstable chemical that decomposes and forms oxygen gas. This decomposition could be illustrated by a series of equations (eqs 1, 2, and 3).

$$H_2O_2 + 2H^+ + 2e^- \rightarrow 2H_2O \quad E° = +1.776 \text{ V} \quad (1)$$

$$H_2O_2 \rightarrow O_2 + 2H^+ + 2e^- \quad E° = -0.682 \text{ V} \quad (2)$$

$$2H_2O_2 \rightarrow O_2 + 2H_2O \quad E° = +1.094 \text{ V} \quad (3)$$

Actually, eq 3 results from the combination of eq 1 and eq 2 and is considered as a proportional reaction in which H_2O_2 undergoes both oxidation to oxygen gas and reduction to water. A series of steps are involved in the formation of the oxygen molecules; however, the kinetics of eq 3 is determined by a rate-determining step, which involves the formation of oxygen atoms. Since these as-formed oxygen atoms are very reactive (and are, therefore, sometimes termed as nascent oxygens), they react readily with either other oxygen atoms or zinc ions on or near the substrate to form molecular oxygen and ZnO coatings, respectively. Heterogeneous nucleation of molecular oxygen is more dominant than homogeneous nucleation thermodynamically, and hence, molecular oxygen gases can be found on solid surfaces and also be bubbled into solutions. There is a competition between the oxygen atoms reacting with $[Zn(H_2O)_6]^{2+}$ ions and those reacting with other remaining oxygen atoms in the next step for continuing the reaction. It is
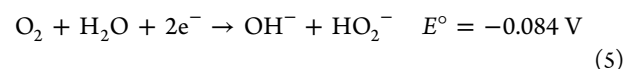
possible that a major portion of the oxygen atoms produced on the Cu micropillar tend to combine directly with $[Zn(H_2O)_6]^{2+}$ ions to grow the ZnO nanocrystals on the substrate surface, while a few of them remain to form molecular oxygen.[39] Hence, as seen in Figure 9, the coatings are comprised of ZnO as the major component (70−77%) and $Zn(OH)_2$ as the minor component (15−25%).

As shown in Figure 9, the composition of the coating revealed a slight decrease in ZnO (i.e., 75.65%, 73.97%, and 70.33%) but a slight increase in Zn−OH (i.e., 18.96%, 22.22%, and 25.80%) with an increase in the H_2O_2 concentration (from 10, 15, and up to 20 mM, respectively) in the baths. In addition to the formation of ZnO during the electrochemical reduction of hydrogen peroxide (as per eqs 1, 2, and 3), there is a possible way to form a small amount of ZnO through the dehydration of $Zn(OH)_2$, which could possibly be precipitated out according to eq 7 in a later stage. With an increase in the H_2O_2 concentration in the bath, the formation of both atomic oxygen and hydroxide ions is bound to improve. The formation of ZnO on the Cu micropillar may be kinetically controlled and lead to a limiting rate; however, the precipitation of $Zn(OH)_2$ may be thermodynamically controlled and enhance the concentration of hydroxide ions. As a result, the amounts of $Zn(OH)_2$ increased slightly in comparison to the amount of ZnO.

This electrochemical formation of ZnO in the presence of hydrogen peroxide has also been observed previously and was termed as "electroprecipitation" by Pauporte and Lincot.[40] As depicted in Figure 10, the ZnO nanorods displayed higher density of intrinsic defects when they were electrochemically deposited in the bath containing H_2O_2 at a higher concentration. This can be understood by the following argument. The reactions depicted in eq 1, eq 2, and eq 3 are thermodynamically inclined to proceed toward the product side with an increase in the H_2O_2 concentration. As a result, oxygen molecules are produced in large amounts on the substrate. Some of them tend to occupy the possible nucleation sites to grow ZnO nanorods, thus hindering the kinetics of the formation of ZnO nanorods and inducing a few defects in the crystals. However, others are dissolved into the solution, which increases the concentration of hydroxide ions marginally, as shown in eq 4.

$$O_2 + 2H_2O + 4e^- \rightarrow 4OH^- \quad E° = +1.229 \text{ V} \quad (4)$$

Equation 4 could be considered as a combination of eq 5 and eq 6.

$$O_2 + H_2O + 2e^- \rightarrow OH^- + HO_2^- \quad E° = -0.084 \text{ V} \quad (5)$$

$$HO_2^- + H_2O + 2e^- \rightarrow 3OH^- \quad E° = +0.870 \text{ V} \quad (6)$$

Consequently, hydroxyl ions are formed at higher concentrations around the Cu micropillar cathode in the baths containing higher concentrations of H_2O_2. Once the solubility product of $[Zn^{2+}][OH^-]^2$ exceeds the Ksp of $Zn(OH)_2$, a precipitation reaction (as shown in eq 7) occurs to form $Zn(OH)_2$.

$$Zn^{2+} + 2OH^- \rightarrow Zn(OH)_2 \quad Ksp = 2.5 \times 10^{-7} \quad (7)$$
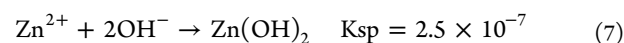
The precipitation of hydroxides facilitates dehydration at temperatures higher than 70 °C, which leads to the production of ZnO crystals, as shown in eq 8.[41]
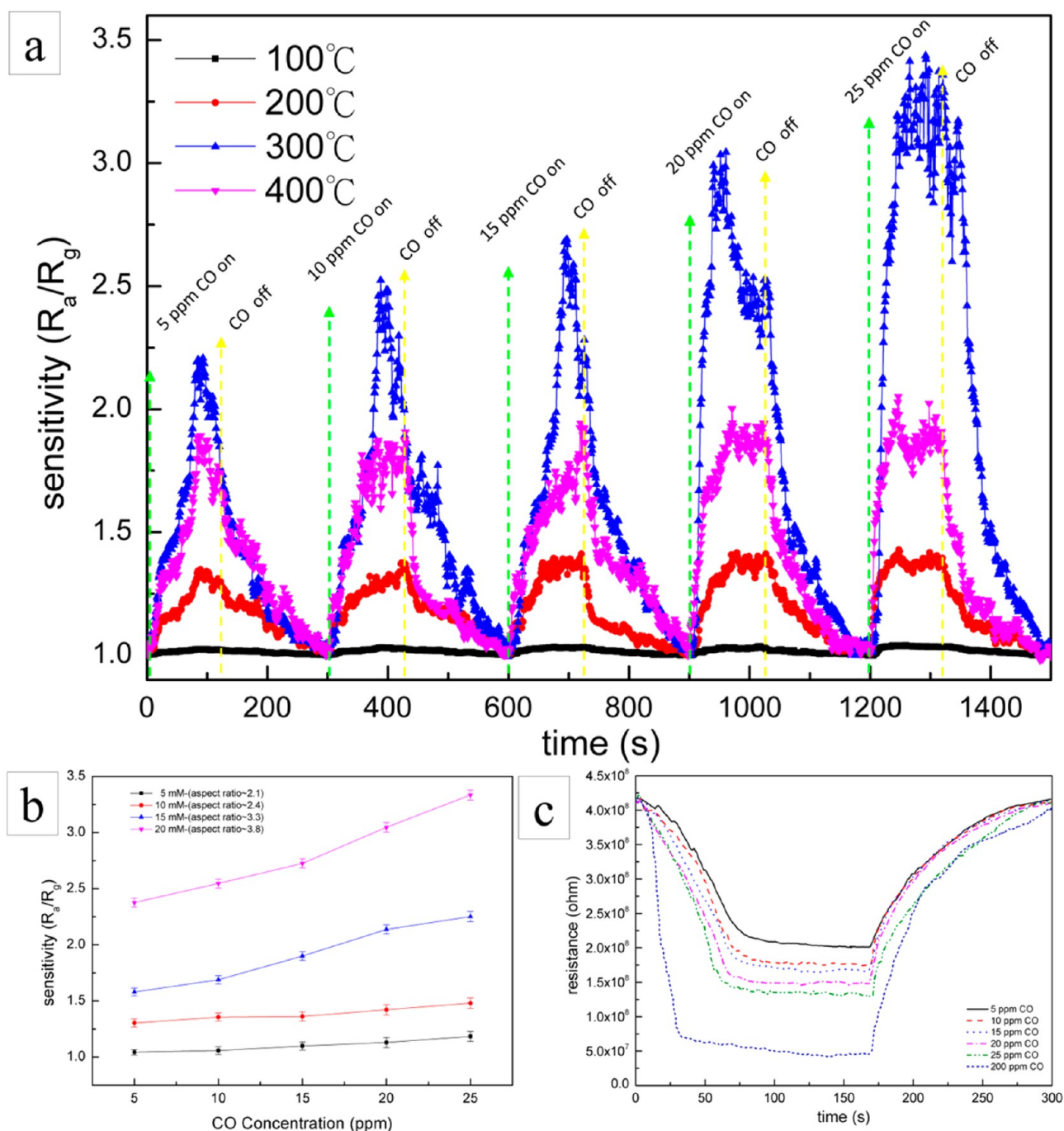
Figure 11. Dynamic sensing response of the sensor to CO gas at 100, 200, 300, and 400 °C by means of (a) ZnO nanorods electrodeposited from a bath containing 2.0 mM $ZnCl_2$ and 20 mM H_2O_2. (b) Dependence of the sensitivity on the concentration of CO for the sensors operated at 300 °C. These sensors were made of different ZnO coatings electrodeposited from a bath containing 2.0 mM $ZnCl_2$ and 5, 10, 15, and 20 mM H_2O_2. (c) Variation of the electrical resistance with time for the sensors operated at 300 °C with a ZnO coating electrodeposited from a bath containing 2.0 mM $ZnCl_2$ and 20 mM H_2O_2. Different concentrations of CO gas (ranging from 5 to 200 ppm) were flown through the furnace for testing.

$$Zn(OH)_2 \rightarrow ZnO + H_2O \qquad (8)$$
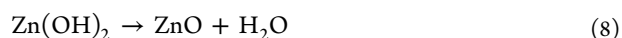
Accordingly, hydroxide ions are inevitably produced at high concentrations in the bath containing concentrated H_2O_2, and then, the reaction equilibrium tends to favor the shift to the product side in eq 7. This trend resulted in a slight increase in $Zn(OH)_2$ content when the electrochemical coating of ZnO was performed in baths with high H_2O_2 concentrations, as depicted in Figure 9.

ZnO nanostructures could be produced on different substrates (i.e., glass, ceramic, and Au-coated Si substrates) without any need for electrochemical sources and hydrogen peroxide (i.e., by hydrothermal process and chemical bath deposition);[42−44] however, these processes take a much longer duration to form the ZnO nanostructures, and their morphologies are dependent on the concentration of zinc and on that of the additives (such as ammonium hydroxide, sodium hydroxide, and hexamine).

11433

dx.doi.org/10.1021/am5019836 | ACS Appl. Mater. Interfaces 2014, 6, 11424−11438
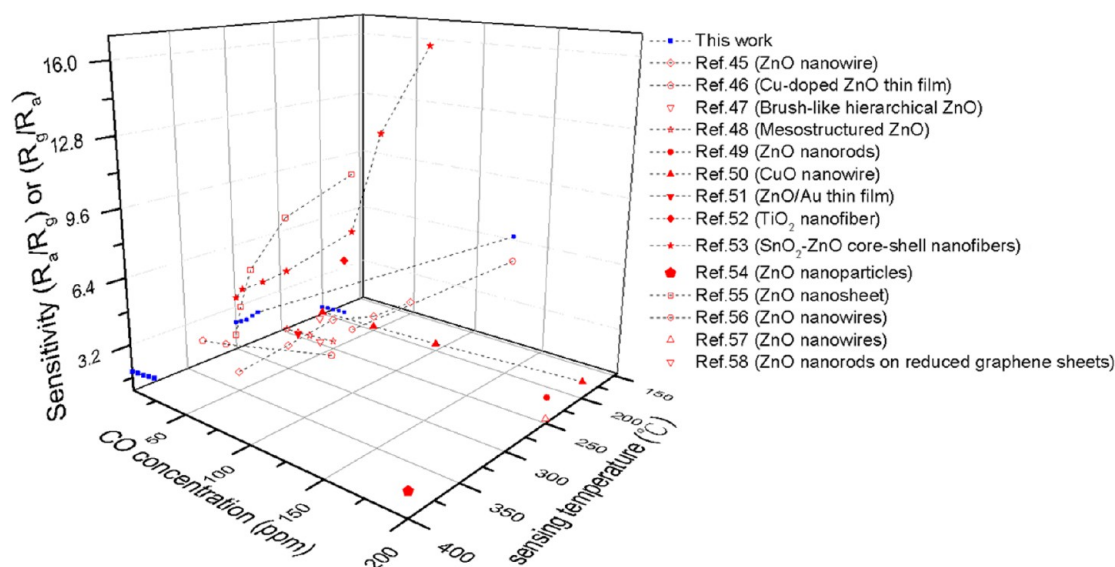
Figure 12. Sensitivity for the microsensor fabricated by ZnO coatings on the crossed Cu micropillars in comparison with that reported in recent published works for performance CO sensing at temperature ranging from 150 to 400 °C with increasing CO concentration from 5 to 200 ppm.

3.7. Dependence of the Sensitivity of the Sensors on the Morphology of ZnO Coatings.

Figure 11(a) displays the dynamic sensing response of a cross-type sensor coated with ZnO nanorods, which were electrochemically deposited using a bath containing 2.0 mM $ZnCl_2$ and 20 mM H_2O_2. A stream of mixed gases with CO contents of 5, 10, 15, 20, and 25 ppm at a flow rate of 500 sccm was made to pass through the tube furnace at 100, 200, 300, and 400 °C to measure the change in the electrical resistance in comparison with the resistance behavior. The performance of the microsensor was tested by cyclic input through periodic on−off profiling (with an on time of 170 s and off time 130 s). As mentioned in Section 2.4, the sensitivity (i.e., S) is defined as the ratio of the electrical resistances (i.e., R_a/R_g) of reducing gases (R_g) and oxidizing gases (R_a). As shown in Figure 11(a), the S value of ZnO coatings for detecting 25 ppm of CO gas increased from 1.04 to 3.43 (i.e., at the highest value) with an increase in the sensing temperature from 100 to 300 °C but decreased to a lower value (i.e., 2.05) at 400 °C. With an increase in the concentration of CO gas from 5 to 25 ppm, S increased for the ZnO coatings operating at a temperature higher than 100 °C. The ZnO coatings showed the highest value of S (i.e., 3.43) for detecting 25 ppm of CO gas when operated at 300 °C. The ZnO coatings demonstrated very good reproducibility when operated at 300 °C.

Referring to the data summarized in Table 1, we found that the L/D of the nanorods increased from 2.1 to 3.8 with increase in the H_2O_2 concentration in the baths used for electrochemical ZnO coating. This indicated that ZnO nanorods with greater L/D were produced from electrochemical baths containing concentrated H_2O_2. Figure 11(b) demonstrates the dependence of S on the concentration of CO gas for ZnO nanorods with various L/Ds in the coating when operated at 300 °C. The higher the L/D of the ZnO nanorods, the higher the S value, especially when the concentration of the CO gas was increased 5 to 25 ppm. The ZnO nanorods with L/D of 3.8 (which were electrochemically deposited from a bath containing 2.0 mM $ZnCl_2$ and 20 mM H_2O_2) showed the best value of S (of 3.34) for 25 ppm of CO gas when operated at 300 °C. It is seems that

the sensitivity of the coatings increases linearly with an increase in the L/Ds of the ZnO nanorods.

It is important to define the response and recovery time to gage and compare the performance of the sensing properties. For a typical sensor, which senses based on differences in electrical resistance, the response time is the duration spent by the sensor on achieving 90% of the total resistance in the adsorption stage beginning from the input of detective gas. The recovery time is the duration for the depletion of 90% of the total resistance during desorption when the gas to be detected is turned off, while the continuous flow of the carrier gas (i.e., air) is maintained. Figure 11(c) shows the sensitivity of the sensors with the reaction time on turning on the input of the CO/air mixture containing CO at various concentrations for 170 s and then turning off the supply of CO gas while keeping the air flow for a duration of 130 s until the next cycle of gas detection. According to the above-mentioned definition, we estimated the data of response and recovery time of the sensors operated at 300 °C. From Figure 11, we found that the response time decreased from 78, 72, 70, 66, 61, to 30 s with an increase in the concentration of CO gas from 5, 10, 15, 20, 25, to 200 ppm; however, the recovery time seemed to increase from 85, 87, 91, 94, 98, and to 107 s, respectively.

There are many different materials that can be used for gas sensing. We are interested in the sensing behavior of the materials depending upon the temperature and CO concentration of the mixed stream varying in CO/air ratios. It is more convenient for comparison by making a conversion of the sensing response from $((R_a - R_g)/(R_a)) \times 100\%$ to $(R_a)/(R_g)$ for n-type semiconducting materials (i.e., ZnO).[45−48] According to the sensitivity evaluated by $(R_a)/(R_g)$ (for n-type materials) and $(R_g)/(R_a)$ (for a p-type semiconductor like CuO), we drew a 3D plot, as depicted in Figure 12 to correlate the sensitivity of the sensing materials with the sensing temperature and CO concentration reported in the recent publications.[45−58] In the sensing temperature ranging from 150 to 400 °C and CO concentration in the range from 5 to 200 ppm, we find that the sensitivity of our microsensor is comparable with those developed in previous studies.
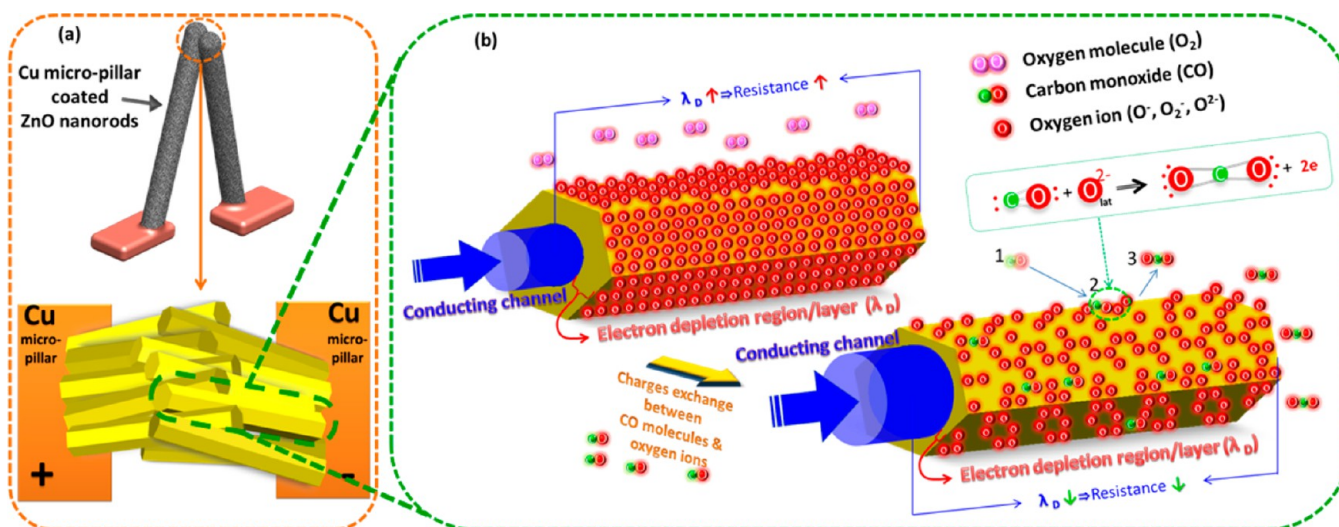
Figure 13. (a) Schematic of the sensor indicating a crossed structure of the Cu micropillars coated with a layer of ZnO nanorods with the contact region magnified. (b) The individual nanorod was heavily adsorbed with oxygen molecules at first to induce a pronounced layer of spacing charges (i.e., thicker layer of electron depletion region), thus decreasing the cross section of the conducting channel for the charge carrier (i.e., electrons in this case). Subsequently, exposing the ZnO nanorod to the CO molecules caused their reaction of CO with oxygen molecules to form CO_2 releasing electrons on the nanorod, which decreased the adsorption of oxygen as well as the thickness of the electron depletion region.
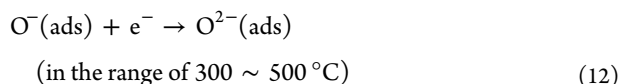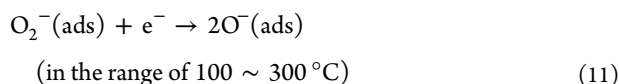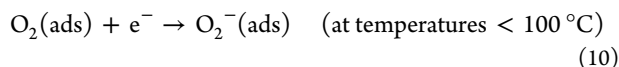
Evidently, the sensitivity of the microsensor fabricated by ZnO nanorods deposited on Cu micropillars is quite good as compared to those in other works.

3.8. Sensing Mechanism of the ZnO Coatings. A typical sensor can be categorized as a resistance-type sensor if it works on the basis of a change in the electrical resistance of the sensing materials upon interaction with the gas to be detected and the oxygen adsorbed. The schematic of the sensor used in this work, which consisted of a crossed structure of Cu micropillars coated with a layer of ZnO nanorods with the contact region magnified, is shown in Figure 13(a). The function of the sensor is shown in Figure 13(a) and (b) by loading a direct current (DC) from one copper electrode through the crossing region to another copper electrode. Under this DC load, the response of the electrical resistance of an individual ZnO nanorod chemisorbed with oxygen prior to sensing and its response after exposure to CO gas are compared schematically in Figure 13(b) to show the area of cross section of the conducting channels for the charge carriers. As depicted in Figure 13(b), when a ZnO nanorod was placed in an open atmosphere, the oxygen adsorbed on the nanorod surface tended to extract electrons from the conduction band, thus forming a depletion region. This depletion region reduces the conducting width of the ZnO nanorod and increases the potential barrier of the contacts between the nanorods and, thereby, increases the resistance of the sensor. It has been reported that the electrical resistance of the nanorod is determined by the nature of its oxygen adsorption, which strongly depends on its crystal structures (especially the defects) and temperatures of adsorption. The Debye length (i.e., the distance over which a localized electric field affects the distribution of free charge carriers) was estimated at 30−35 nm according to previous studies.[59,60] The ZnO nanorods in the electrochemical coating showed almost the same size as observed in the previous reports. Therefore, the surface depletion of charges caused by oxygen adsorption will greatly influence the density and mobility of the electrons in the nanorods. For ZnO nanorods with comparable radius, in light of their Debye length in air atmosphere, an adsorption of

oxygen species (electron acceptor) to form oxygen ions (O^-, O^{2-}, or O_2^-) on the surface of the ZnO nanorods leads to a shift in the Fermi level away from the conduction band. In contrast, under air atmosphere, the possible presence of oxygen vacancies makes ZnO nanorods behave as an n-type semi-conductors. As a result, the pronounced adsorption of oxygen species causes a thicker zone of charge-depleted region (CDR) inside the ZnO nanorods in air atmosphere in comparison to the possible oxygen vacancies present, thus decreasing the thickness of the CDR in the atmosphere of the CO/air mixture.[61] The ZnO nanorods in the coating with greater CDR thickness result in a lower current (hence, the resistance increases) in sensors operated in air atmosphere at a constant voltage loaded with DC. In contrast, the ZnO nanorods with less thick CDR lead to a greater current (and a lower resistance) in sensors operated in an atmosphere of CO/air gas mixture. Referring to the literature, the sites available for oxygen adsorption are determined by the concentration of oxygen vacancies on the ZnO crystal surface.[49] The more concentrated the oxygen vacancies on the ZnO nanostructure, the higher the number of chemisorption sites present. The PL spectra shown in Figure 10 (as discussed before in Section 3.5) exhibited a higher intensity of visible-light emissions in response to an increase in the oxygen vacancies on the ZnO nanorods and resulted in an increase in the sensitive sites, and therefore, the value of S increased.

Prior to exposing the sensor to the gas for detection, oxygen plays an important role as the electron acceptor by trapping electrons from the conductive band and then generates a surface depletion region, increasing the resistance. The chemisorption of oxygen depends on thermal conditions, and different oxygen species chemisorb on the ZnO nanorods. For example, adsorption of O_2^- takes place at temperatures <100 °C; adsorption of O^- occurs in the range of 100−300 °C; and the adsorption of O^{2-} occurs in the range 300−500 °C. The corresponding reaction kinetics can expressed as follows.[49,62,63]

$$O_2(gas) \rightarrow O_2(ads) \qquad (9)$$

$$O_2(ads) + e^- \rightarrow O_2^-(ads) \quad \text{(at temperatures} < 100\,°C)$$
(10)

$$O_2^-(ads) + e^- \rightarrow 2O^-(ads)$$
$$\text{(in the range of } 100 \sim 300\,°C)$$
(11)

$$O^-(ads) + e^- \rightarrow O^{2-}(ads)$$
$$\text{(in the range of } 300 \sim 500\,°C)$$
(12)

According to the chemisorption of oxygen species on the ZnO nanorod, the extraction of electrons induces a depletion region of electrons in the nanorod to hinder the mobility of the charge carriers. Therefore, an n-type ZnO nanorod chemisorbed with oxygen results in an increase in the electrical resistance prior to the sensing of CO gas.

In the process of CO sensing, the ZnO nanorods are exposed to a gas mixture of CO and air. The CO molecules are subjected to reaction with oxygen ions according to the following equations.[50,64]

$$CO + \frac{1}{2}O_2^-(ads) \rightarrow CO_2(gas) + \frac{1}{2}e^-$$
(13)

$$CO + O^-(ads) \rightarrow CO_2(gas) + e^-$$
(14)

$$CO + O^{2-}(ads) \rightarrow CO_2(gas) + 2e^-$$
(15)
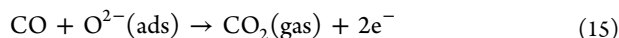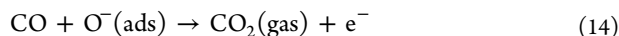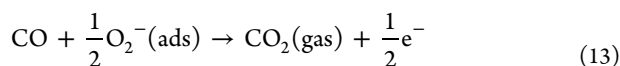
According to eq 13, eq 14, and eq 15, the CO molecules react with all three oxygen species to some extent and release some of the electrons extracted by the chemisorbed oxygen. This release of electrons could mitigate the depletion of electrons and decrease the thickness of the depletion ring inside the ZnO nanorod. Consequently, the cross section of the nanorods could provide a greater volume of conducting channels to accelerate the mobility of the electrons and hence decrease the resistance.

It is known that the sensing properties of a nanostructured metal oxide depend upon the geometry, aspect ratio, and the type of the nanostructure.[65] In this work, the sensing elements, i.e., the ZnO nanorods, were vertically aligned in the coatings and were closely in contact with each other at the crossing region of the sensor. As depicted earlier in Figure 11(b) (in Section 3.7), the sensor comprised of ZnO nanorods with higher L/D gave rise to higher S values. This could be understood based on the following mechanism we propose. A sensor coated with ZnO nanorods with higher L/D possesses a greater surface area for oxygen adsorption, and the individual ZnO nanorods of the depletion region cross each other significantly. As a result, the ZnO nanorods with higher L/Ds provide more sensing sites than those with lower L/Ds. Indeed, the results obtained in the present study were in good agreement with other previous studies.[45,66]

The sensitivity of the resistance-type sensors is believed to involve a complicated phenomenon determined by three factors: (i) adsorption reactions on the surface, (ii) mechanism of charge transport for the carriers within the sensing layer, and (iii) thermodynamics and kinetics of adsorption and desorption.[67,68] The effect of temperature on the sensitivity of the sensors could also be understood based on the mechanism proposed. In Figure 11(a), we found that the sensor shows the best S value at 300 °C, and the S value decreased in the following order: 300 > 400 > 200 > 100 °C. The unexpected lower S value at 400 °C is of interest. There is

little doubt that the degree of oxygen chemisorption is thermally dependent in accordance with eq 10, eq 11, and eq 12, and additional $O^{2-}(ads)$ species were chemisorbed at 400 °C in comparison to the adsorption of species, such as $O_2(ads)$, $O_2^-(ads)$, and $O^-(ads)$ at 300 °C. In the subsequent stage, when CO gas was introduced, the detected CO molecules tended to react with the different oxygen species chemisorbed on the ZnO nanorods according to eq 13, eq 14, and eq 15. The overall process of the reaction has been reported to be exothermic.[46,69] Referring to thermodynamics, the exothermic reaction is not favored to proceed with an increase in the reaction temperatures, especially at the higher degree of adsorption of $O^{2-}(ads)$ species on the ZnO nanorods at temperatures higher than 300 °C. As a result, the maximum S value of the sensor was achieved at a critical temperature of ~300 °C. This is consistent with results reported by other studies on the sensing properties of ZnO nanostructures.

4. CONCLUSION

A novel microsensor consisting of two Cu micropillars coated with well-aligned ZnO nanorods fabricated into a cross shape was successfully obtained by electrochemical processing. This sensor provided a sensitive response to CO gas, and the sensitivity depended on the morphology of the coatings of the ZnO nanorods resulting from the electrochemical baths with varying hydrogen peroxide concentrations. Better sensitivity of detection of CO gas with concentration increased from 5 to 25 ppm (from 2.22 to 3.43 at 300 °C) was achieved for the sensor coated with ZnO nanorods of a higher L/D (i.e., 3.8) obtained from an electrochemical bath containing 20 mM H_2O_2. XPS analysis demonstrated that the chemical states ZnO and $Zn(OH)_2$ were responsible for the sensing. The analysis of the PL spectra indicated that the intrinsic defects of oxygen vacancies contributed to a slight increase in the sensitivity. A thermal effect was observed on the sensitivity, and the best sensitivity was achieved at 300 °C. The mechanisms operating behind the electrochemical coating and the sensing of CO gas are proposed in the article.

■ AUTHOR INFORMATION

Corresponding Author
*Tel.: +886-3-426-7328. Fax: +886-3-425-4501. E-mail: jclincom@cc.ncu.edu.tw.

Notes
The authors declare no competing financial interest.

■ ACKNOWLEDGMENTS

■ REFERENCES

(1) Lin, J. C.; Yang, J. H.; Chang, T. K.; Jiang, S. B. On the Structure of Micrometer Copper Features Fabricated by Intermittent Micro-Anode Guided Electroplating. *Electrochim. Acta* **2009**, *54*, 5703−5708.

(2) Lin, J. C.; Chang, T. K.; Yang, J. H.; Chen, Y. S.; Chuang, C. L. Localized Electrochemical Deposition of Micrometer Copper Columns by Pulse Plating. *Electrochim. Acta* **2010**, *55*, 1888−1894.

(3) Chen, Y. S.; Lin, J. C.; Lin, Z. H.; Li, C.; Chang, J. K. Effect of Solvent on the Morphology of Nickel Localized Electrochemical Deposition. *J. Electrochem. Soc.* **2011**, *158*, D264−D268.

(4) Lin, J. C.; Chang, T. K.; Yang, J. H.; Jeng, J. H.; Lee, D. L.; Jiang, S. B. Fabrication of A Micrometer Ni−Cu Alloy Column Coupled with a Cu Micro-Column for Thermal Measurement. *J. Micromech. Microeng.* **2009**, *19*, 015030.

(5) Hong, W. K.; Sohn, J. I.; Hwang, D. K.; Kwon, S. S.; Jo, G.; Song, S.; Kim, S. M.; Ko, H. J.; Park, S. J.; Welland, M. E.; Lee, T. Tunable Electronic Transport Characteristics of Surface-Architecture-Controlled ZnO Nanowire Field Effect Transistors. *Nano Lett.* **2008**, *8*, 950−956.

(6) Kim, Y. H.; Kim, J. S.; Kim, W. M.; Seong, T. Y.; Lee, J.; Müller-Meskamp, L.; Leo, K. Realizing the Potential of ZnO with Alternative Non-Metallic Co-Dopants as Electrode Materials for Small Molecule Optoelectronic Devices. *Adv. Funct. Mater.* **2013**, *23*, 3645−3652.

(7) Heo, Y. W.; Tien, L. C.; Norton, D. P.; Kang, B. S.; Ren, F.; Gila, B. P.; Pearton, S. J. Electrical Transport Properties of Single ZnO Nanorods. *Appl. Phys. Lett.* **2004**, *85*, 2002−2004.

(8) Hernandez-Ramirez, F.; Prades, J. D.; Jimenez-Diaz, R.; Fischer, T.; Romano-Rodriguez, A.; Mathur, S.; Morante, J. R. On the Role of Individual Metal Oxide Nanowires in the Scaling Down of Chemical Sensors. *Phys. Chem. Chem. Phys.* **2009**, *11*, 7105−7110.

(9) Chen, L.; Liu, Z.; Bai, S.; Zhang, K.; Li, D.; Chen, A.; Liu, C. C. Synthesis of 1-Dimensional ZnO and Its Sensing Property for CO. *Sens. Actuators, B* **2010**, *143*, 620−628.

(10) Weintraub, B.; Zhou, Z.; Li, Y.; Deng, Y. Solution Synthesis of One-Dimensional ZnO Nanomaterials and Their Applications. *Nanoscale* **2010**, *2*, 1573−1587.

(11) Chang, S. J.; Hsueh, T. J.; Hsu, C. L.; Lin, Y. R.; Chen, I. C.; Huang, B. R. A ZnO Nanowire Vacuum Pressure Sensor. *Nanotechnology* **2008**, *19*, 095505.

(12) Wu, L.; Song, F.; Fang, X.; Guo, Z. X.; Liang, S. A Practical Pacuum Sensor Based on a ZnO Nanowire Array. *Nanotechnology* **2010**, *21*, 475502.

(13) Kim, I.; Rothschild, A.; Yang, D.; Tuller, H. Macroporous TiO₂ Thin Film Gas Sensors Obtained Using Colloidal Templates. *Sens. Actuators, B* **2008**, *130*, 9−13.

(14) Barreca, D.; Bekermann, D.; Comini, E.; Devi, A.; Fischer, R. A.; Gasparotto, A.; Maccato, C.; Sberveglieri, G.; Tondello, E. 1D ZnO Nano-Assemblies by Plasma-CVD as Chemical Sensors for Flammable and Toxic Gases. *Sens. Actuators, B* **2010**, *149*, 1−7.

(15) Du, X.; Du, Y.; George, S. M. CO Gas Sensing by Ultrathin Tin Oxide Films Grown by Atomic Layer Deposition Using Transmission FTIR Spectroscopy. *J. Phys. Chem. A* **2008**, *112*, 9211−9219.

(16) Lee, H. U.; Ahn, K.; Lee, S. J.; Kim, J. P.; Kim, H. G.; Jeong, S. Y.; Cho, C. R. ZnO Nanobarbed Fibers: Fabrication, Sensing NO₂ Gas, and Their Sensing Mechanism. *Appl. Phys. Lett.* **2011**, *98*, 193114.

(17) Ramgir, N. S.; Sharma, P. K.; Datta, N.; Kaur, M.; Debnath, A. K.; Aswal, D. K.; Gupta, S. K. Room Temperature H₂S Sensor Based on Au Modified ZnO Nanowires. *Sens. Actuators, B* **2013**, *186*, 718−726.

(18) Williams, D. E. Semiconducting Oxides as Gas-Sensitive Resistors. *Sens. Actuators, B* **1999**, *57*, 1−16.

(19) Gurlo, A.; Riedel, R. In Situ and Operando Spectroscopy for Assessing Mechanisms of Gas Sensing. *Angew. Chem., Int. Ed.* **2007**, *46*, 3826−3848.

(20) Pauporté, T.; Lincot, D. Hydrogen Peroxide Oxygen Precursor for Zinc Oxide Electrodeposition I. Deposition in Perchlorate Medium. *J. Electrochem. Soc.* **2001**, *148*, C310−C314.

(21) Williams, D. B., Carter, C. Barry *Transmission Electron Microscopy: A Textbook for Materials Science*, 2nd ed.; Springer US: New York, 2009; p 760.

(22) Fahoume, M.; Maghfoul, O.; Aggour, M.; Hartiti, B.; Chraïbi, F.; Ennaoui, A. Growth and Characterization of ZnO Thin Films Prepared by Electrodeposition Technique. *Sol. Energy Mater. Sol. Cells* **2006**, *90*, 1437−1444.

(23) Yang, C.; Xu, C. X.; Wang, X. M. ZnO/Cu Nanocomposite: A Platform for Direct Electrochemistry of Enzymes and Biosensing Applications. *Langmuir* **2012**, *28*, 4580−4585.

(24) Chen, M.; Wang, Z. H.; Han, D. M.; Gu, F. B.; Guo, G. S. Porous ZnO Polygonal Nanoflakes: Synthesis, Use in High-Sensitivity

NO₂ Gas Sensor, and Proposed Mechanism of Gas Sensing. *J. Phys. Chem. C* **2011**, *115*, 12763−12773.

(25) Nicholas, N. J.; Franks, G. V.; Ducker, W. A. The Mechanism for Hydrothermal Growth of Zinc Oxide. *CrystEngComm* **2012**, *14*, 1232.

(26) McCluskey, M. D.; Jokela, S. J. Defects in ZnO. *J. Appl. Phys.* **2009**, *106*, 071101.

(27) Janotti, A.; Van de Walle, C. G. Native Point Defects in ZnO. *Phys. Rev. B: Condens. Matter Mater. Phys.* **2007**, *76*, 165202.

(28) Lee, M. K.; Tu, H. F. Ultraviolet Emission Blueshift of ZnO Related to Zn. *J. Appl. Phys.* **2007**, *101*, 126103.

(29) Wei, X. Q.; Zhang, Z.; Yu, Y. X.; Man, B. Y. Comparative Study on Structural and Optical Properties of ZnO Thin Films Prepared by PLD Using ZnO Powder Target and Ceramic Target. *Opt. Laser Technol.* **2009**, *41*, 530−534.

(30) Cheng, W.; Wu, P.; Zou, X.; Xiao, T. Study on Synthesis and Blue Emission Mechanism of ZnO Tetrapodlike Nanostructures. *J. Appl. Phys.* **2006**, *100*, 054311.

(31) Wei, X. Q.; Man, B. Y.; Liu, M.; Xue, C. S.; Zhuang, H. Z.; Yang, C. Blue Luminescent Centers and Microstructural Evaluation by XPS and Raman in ZnO Thin Films Annealed in Vacuum, N₂ and O₂. *Phys. B* **2007**, *388*, 145−152.

(32) Srikant, V.; Clarke, D. R. On the Optical Band Gap of Zinc Oxide. *J. Appl. Phys.* **1998**, *83*, 5447−5451.

(33) Look, D. C.; Hemsky, J. W.; Sizelove, J. R. Residual Native Shallow Donor in ZnO. *Phys. Rev. Lett.* **1999**, *82*, 2552−2555.

(34) Zeng, H.; Duan, G.; Li, Y.; Yang, S.; Xu, X.; Cai, W. Blue Luminescence of ZnO Nanoparticles Based on Non-Equilibrium Processes: Defect Origins and Emission Controls. *Adv. Funct. Mater.* **2010**, *20*, 561−572.

(35) Huang, M. H.; Wu, Y.; Feick, H.; Tran, N.; Weber, E.; Yang, P. Catalytic Growth of Zinc Oxide Nanowires by Vapor Transport. *Adv. Mater.* **2001**, *13*, 113−116.

(36) Shalish, I.; Temkin, H.; Narayanamurti, V. Size-Dependent Surface Luminescence in ZnO Nanowires. *Phys. Rev. B: Condens. Matter Mater. Phys.* **2004**, *69* (24), 245401.

(37) Djurisic, A. B.; Leung, Y. H. Optical Properties of ZnO Nanostructures. *Small* **2006**, *2*, 944−961.

(38) Sun, Y.; Ashfold, M. N. R. Photoluminescence from Diameter-Selected ZnO Nanorod Arrays. *Nanotechnology* **2007**, *18*, 245701.

(39) Singh, N.; Mittal, S.; Sood, K.; Gupta, P. Controlling the Flow of Nascent Oxygen Using Hydrogen Peroxide Results in Controlling the Synthesis of ZnO/ZnO₂. *Chalcogenide Lett.* **2010**, *7*, 275−281.

(40) Pauporté, T.; Lincot, D. Hydrogen Peroxide Oxygen Precursor for Zinc Oxide Electrodeposition II—Mechanistic Aspects. *J. Electroanal. Chem.* **2001**, *517*, 54−62.

(41) Ramirez, D.; Bartlett, P.; Abdelsalam, M.; Gomez, H.; Lincot, D. Electrochemical Synthesis of Macroporous Zinc Oxide Layers by Employing Hydrogen Peroxide as Oxygen Precursor. *Phys. Status Solidi A* **2008**, *205*, 2365−2370.

(42) Yan, X.; Li, Z.; Chen, R.; Gao, W. Template Growth of ZnO Nanorods and Microrods with Controllable Densities. *Cryst. Growth Des.* **2008**, *8*, 2406−2410.

(43) Edri, E.; Rabinovich, E.; Niitsoo, O.; Cohen, H.; Bendikov, T.; Hodes, G. Uniform Coating of Light-Absorbing Semiconductors by Chemical Bath Deposition on Sulfide-Treated ZnO Nanorods. *J. Phys. Chem. C* **2010**, *114*, 13092−13097.

(44) Chen, D. W.; Wang, T. C.; Liao, W. P.; Wu, J. J. Synergistic Effect of Dual Interfacial Modifications with Room-Temperature-Grown Epitaxial ZnO and Adsorbed Indoline Dye for ZnO Nanorod Array/P3HT Hybrid Solar Cell. *ACS Appl. Mater. Interfaces* **2013**, *5*, 8359−8365.

(45) Chang, S. J.; Hsueh, T. J.; Chen, I. C.; Huang, B. R. Highly Sensitive ZnO Nanowire CO Sensors with the Adsorption of Au Nanoparticles. *Nanotechnology* **2008**, *19*, 175502.

(46) Liu, C. Y.; Chen, C. F.; Leu, J. P. Fabrication and CO Sensing Properties of Mesostructured ZnO Gas Sensors. *J. Electrochem. Soc.* **2009**, *156*, J16−J19.

11437

dx.doi.org/10.1021/am5019836 | *ACS Appl. Mater. Interfaces* 2014, 6, 11424−11438

(47) Hung, N. L.; Kim, H.; Hong, S. K.; Kim, D. Enhancement of CO Gas Sensing Properties in ZnO Thin Films Deposited on Self-Assembled Au Nanodots. *Sens. Actuators, B* **2010**, *151*, 127−132.

(48) Park, W. J.; Choi, K. J.; Kim, M. H.; Koo, B. H.; Lee, J. L.; Baik, J. M. Self-Assembled and Highly Selective Sensors Based on Air-Bridge-Structured Nanowire Junction Arrays. *ACS Appl. Mater. Interfaces* **2013**, *5*, 6802−6807.

(49) Gong, H.; Hu, J. Q.; Wang, J. H.; Ong, C. H.; Zhu, F. R. Nano-Crystalline Cu-Doped ZnO Thin Film Gas Sensor for CO. *Sens. Actuators, B* **2006**, *115*, 247−251.

(50) Zhang, Y.; Xu, J. Q.; Xiang, Q.; Li, H.; Pan, Q. Y.; Xu, P. C. Brush-Like Hierarchical ZnO Nanostructures: Synthesis, Photoluminescence and Gas Sensor Properties. *J. Phys. Chem. C* **2009**, *113*, 3430−3435.

(51) Wang, J. X.; Sun, X. W.; Yang, Y.; Huang, H.; Lee, Y. C.; Tan, O. K.; Vayssieres, L. Hydrothermally Grown Oriented ZnO Nanorod Arrays for Gas Sensing Applications. *Nanotechnology* **2006**, *17*, 4995−4998.

(52) Liao, L.; Zhang, Z.; Yan, B.; Zheng, Z.; Bao, Q. L.; Wu, T.; Li, C. M.; Shen, Z. X.; Zhang, J. X.; Gong, H.; Li, J. C.; Yu, T. Multifunctional CuO Nanowire Devices: P-type Field Effect Transistors and CO Gas Sensors. *Nanotechnology* **2009**, *20*, 085203.

(53) Park, J. A.; Moon, J. h.; Lee, S. J.; Kim, S. H.; Zyung, T. H.; Chu, H. Y. Structure and CO Gas Sensing Properties of Electrospun TiO_2 Nanofibers. *Mater. Lett.* **2010**, *64*, 255−257.

(54) Park, J. Y.; Choi, S. W.; Kim, S. S. A Model for the Enhancement of Gas Sensing Properties in SnO_2−ZnO Core−Shell Nanofibres. *J. Phys. D: Appl. Phys.* **2011**, *44*, 205403.

(55) Rai, P.; Yu, Y. T. Citrate-Assisted Hydrothermal Synthesis of Single Crystalline ZnO Nanoparticles for Gas Sensor Application. *Sens. Actuators, B* **2012**, *173*, 58−65.

(56) Zeng, Y.; Qiao, L.; Bing, Y.; Wen, M.; Zou, B.; Zheng, W.; Zhang, T.; Zou, G. Development of Microstructure CO Sensor Based on Hierarchically Porous ZnO Nanosheet Thin Films. *Sens. Actuators, B* **2012**, *173*, 897−902.

(57) Rai, P.; Khan, R.; Ahmad, R.; Hahn, Y. B.; Lee, I. H.; Yu, Y. T. Gas Sensing Properties of Single Crystalline ZnO Nanowires Grown by Thermal Evaporation Technique. *Curr. Appl. Phys.* **2013**, *13*, 1769−1773.

(58) Zou, R. J.; He, G. J.; Xu, K. B.; Liu, Q.; Zhang, Z. Y.; Hu, J. Q. ZnO Nanorods on Reduced Graphene Sheets with Excellent Field Emission, Gas Sensor and Photocatalytic Properties. *J. Mater. Chem. A* **2013**, *1*, 8445−8452.

(59) Lupan, O.; Chow, L.; Pauporté, T.; Ono, L. K.; Roldan Cuenya, B.; Chai, G. Highly Sensitive and Selective Hydrogen Single-Nanowire Nanosensor. *Sens. Actuators, B* **2012**, *173*, 772−780.

(60) Kumar, N.; Srivastava, A. K.; Nath, R.; Gupta, B. K.; Varma, G. D. Probing the Highly Efficient Room Temperature Ammonia Gas Sensing Properties of a Luminescent ZnO Nanowire Array Prepared via An AAO-Assisted Template Route. *Dalton Trans.* **2014**, 5713−5720.

(61) Hongsith, N.; Wongrat, E.; Kerdcharoen, T.; Choopun, S. Sensor Response Formula for Sensor Based on ZnO Nanostructures. *Sens. Actuators, B* **2010**, *144*, 67−72.

(62) Barsan, N.; Weimar, U. Conduction Model of Metal Oxide Gas Sensors. *J. Electroceram.* **2001**, *7*, 143−167.

(63) Della Gaspera, E.; Guglielmi, M.; Martucci, A.; Giancaterini, L.; Cantalini, C. Enhanced Optical and Electrical Gas Sensing Response of Sol−Gel Based NiO−Au and ZnO−Au Nanostructured Thin Films. *Sens. Actuators, B* **2012**, *164*, 54−63.

(64) Kolmakov, A.; Zhang, Y.; Cheng, G.; Moskovits, M. Detection of CO and O_2 Using Tin Oxide Nanowire Sensors. *Adv. Mater.* **2003**, *15*, 997−1000.

(65) Gurav, K. V.; Gang, M. G.; Shin, S. W.; Patil, U. M.; Deshmukh, P. R.; Agawane, G. L.; Suryawanshi, M. P.; Pawar, S. M.; Patil, P. S.; Lokhande, C. D.; Kim, J. H. Gas Sensing Properties of Hydrothermally Grown ZnO Nanorods with Different Aspect Ratios. *Sens. Actuators, B* **2014**, *190*, 439−445.

(66) Chang, J. F.; Kuo, H. H.; Leu, I. C.; Hon, M. H. The Effects of Thickness and Operation Temperature on ZnO:Al Thin Film CO Gas Sensor. *Sens. Actuators, B* **2002**, *84*, 258−264.

(67) Kolmakov, A.; Moskovits, M. Chemical Sensing and Catalysis by One-Dimensional Metal-Oxide Nanostructures. *Annu. Rev. Mater. Res.* **2004**, *34*, 151−180.

(68) Gurlo, A. Nanosensors: Towards Morphological Control of Gas Sensing Activity. SnO_2, In_2O_3, ZnO and WO_3 Case Studies. *Nanoscale* **2011**, *3*, 154−165.

(69) Wang, C.; Yin, L.; Zhang, L.; Qi, Y.; Lun, N.; Liu, N. Large Scale Synthesis and Gas-Sensing Properties of Anatase TiO_2 Three-Dimensional Hierarchical Nanostructures. *Langmuir* **2010**, *26*, 12841−12848.